Complex magnetohydrodynamic bow shock topology in field-aligned low-β flow around a perfectly conducting cylinder

H. De Sterck[a] and B. C. Low
High Altitude Observatory, National Center for Atmospheric Research, P.O. Box 3000, Boulder, Colorado 80307-3000

S. Poedts[b]
Centre for Plasma Astrophysics, Katholieke Universiteit Leuven, Celestijnenlaan 200B, 3001 Leuven, Belgium

(Received 10 March 1998; accepted 27 July 1998)

Two-dimensional ideal magnetohydrodynamic (MHD) simulations are presented that demonstrate several novel phenomena in MHD shock formation. The stationary symmetrical flow of a uniform, planar, field-aligned, low-β and superfast magnetized plasma around a perfectly conducting cylinder is calculated. The velocity of the incoming flow is chosen such that the formation of fast switch-on shocks is possible. Using a time marching procedure, a stationary bow shock is obtained, composed of two consecutive interacting shock fronts. The leading shock front has a dimpled shape and is composed of fast, intermediate and hydrodynamic shock parts. A second shock front follows the leading front. Additional intermediate shocks and tangential discontinuities are present in the downstream part of the flow. The intermediate shocks are of the 1–3, 1–4, 2–4 and 1=2–3=4 types. This is a confirmation in two dimensions of recent results on the admissibility of these types of shocks. Recently it has also been shown that the 1=2–3=4 shock, embedded in a double compound wave, is present in the analytical solution of some planar one-dimensional MHD Riemann problems. This MHD flow with interacting shocks may have applications for some observed features of fast solar Coronal Mass Ejections and other phenomena in low-β space plasmas. © *1998 American Institute of Physics.* [S1070-664X(98)00611-9]

I. INTRODUCTION

Bow shocks can be found in many places in the solar system. They are formed when a supersonic flow encounters an obstructing object. The space physics literature on hydrodynamic (HD) and magnetohydrodynamic (MHD) bow shocks is quite extensive. Rankine–Hugoniot (RH) relations quantify the jumps across the shock, and methods exist for the determination of the Mach cone angle, standoff distance, pressure at the object, etc.[1] Analytical solutions of the flow equations are generally impossible to obtain, so numerical simulations are necessary to construct the model solutions for various parameter regimes. Many simulations have been done describing the bow shocks in front of unmagnetized planets (like Venus), magnetized planets (like the Earth), comets, and the sun.[2–7] In these two-dimensional (2D) and three-dimensional (3D) simulations, many different parameter regimes have been explored: high or low plasma β (β being the ratio of the thermal pressure and the magnetic pressure), various orientations of the magnetic field to the plasma velocity, etc. The classical picture of a steady state HD or MHD bow shock is a single-front structure with a concave-inward (to the object) geometrical shape (Fig. 1a).

When the plasma β of the incoming flow is roughly smaller than one and, along the magnetic field lines, the incoming velocity lies between the fast MHD wave speed and roughly twice this speed, fast MHD switch-on shocks are possible.[8] MHD flows with shocks in this parameter regime (which we will call the switch-on regime) have been studied by Steinolfson and Hundhausen[9,10] in the context of fast Coronal Mass Ejections (CMEs) propagating outward from the sun through the low-β inner solar corona. They predicted a ''dimpling'' of the shock front (Fig. 1b). Aspects of their theoretical analysis were confirmed by time-dependent numerical simulations of propagating shock fronts, and supported by coronagraph observations of fast CMEs with a dimpled leading front (which can be interpreted as the signature of a shock front).[11,9] The stationary bow shock in the switch-on regime has not been studied before, apart from one preliminary study with low resolution.[4]

In this paper we study the 2D steady state MHD bow shock for field-aligned flow in the switch-on regime (field-aligned flow is sometimes also called parallel flow). We calculate the flow of a 2D ($\partial/\partial z=0$), uniform, planar ($v_z=B_z=0$), field-aligned, low-β and superfast magnetized plasma around a perfectly conducting cylinder. We look for a stationary flow solution with top–bottom symmetry,[9,10] such that the horizontal line which extends to the center of the cylinder is the stagnation streamline, parallel to the incoming flow (Fig. 1). We obtain a stationary bow shock by using a time marching procedure. In Fig. 2 we show a global

[a]Research Assistant of the Fund for Scientific Research—Flanders (Belgium). Also at the Centre for Plasma Astrophysics, Katholieke Universiteit Leuven, Belgium. Electronic mail: desterck@ucar.edu
[b]Research Associate of the Fund for Scientific Research—Flanders (Belgium).

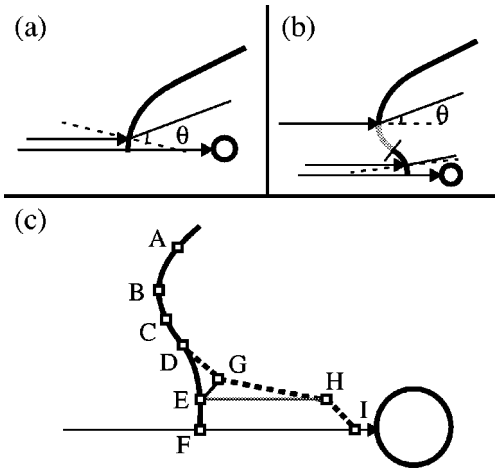

FIG. 1. Possible bow shock topologies for a uniform flow (magnetic field lines have arrows) coming in from the left and obstructed by a conducting cylinder. Shock normals are shown as dashed lines. The horizontal field line terminating on the cylinder is the stagnation streamline. (a) Concave-inward (to the cylinder) shape. The whole shock front (thick line) is of the fast type. (b) Dimpled shape. The upper part of the front is of the fast type. At the nose, a switch-on shock refracts the horizontal incoming magnetic field with a finite angle θ. Under the nose the shock is first of the 1–3 intermediate type, which is then linked to a 1–4 intermediate shock part. (c) Interacting shock topology of our simulation results. The dimple is still present. A–B is a fast shock. B–C–D is of the intermediate type. D–E is fast and E–F is hydrodynamic. The leading front is trailed by an intermediate front D–G–H–I. E–G is another intermediate shock. E–H is a tangential discontinuity.

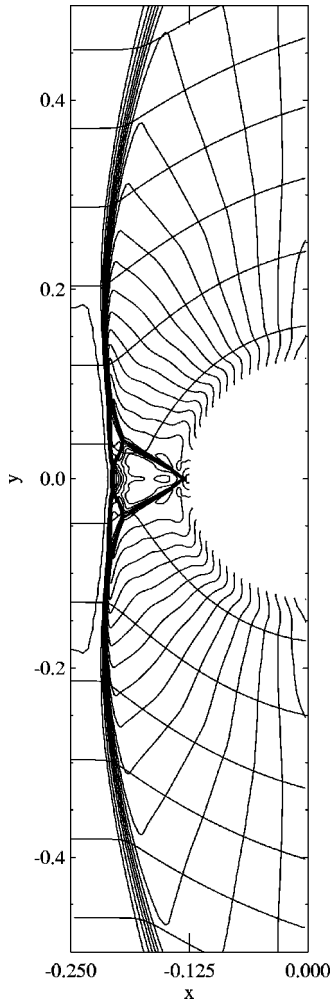

FIG. 2. Global view of the bow shock solution presented in this paper (inflow Mach numbers $M_A=1.5$ and $M=1.5\sqrt{3}$ and $\beta=0.4$). We show density contours (piling up in the shocks) and magnetic field lines (coming in horizontally on the left). The flow comes in from the left. The cylinder fills the space of the white half disc on the right. The leading shock front is slightly dimpled. The upper and lower parts of this front are of the fast type. In the central part of the flow, a second front has separated and is trailing the leading front. Additional discontinuities can be seen in the central interaction region.

view of our simulation results. It is clear that the bow shock in this switch-on regime does not have the traditional geometrical shape and topology of Fig. 1a. It contains a central concave-outward part (''dimple''), confirming this aspect of the analysis of Steinolfson and Hundhausen.[9,10] However, the resulting bow shock flow is quite more complicated than could be anticipated from the important earlier work of Steinolfson and Hundhausen. The leading shock front is followed by a second shock front, and other discontinuities can be identified between the two fronts. This flow pattern may seem intricate and complicated at first. The topology of the flow pattern is sketched in Fig. 1c. In this paper we will propose a consistent interpretation of this flow pattern, and we will explain why we obtain such a complicated flow in our simulation, and not the classical simple concave-inward bow shock topology of Fig. 1a.

We will start with a brief review of the classification of MHD discontinuities in Sec. II, discussing the properties of the different types of MHD discontinuities. This review will help us with the interpretation of our simulation results. In Sec. III we will describe the setup of the simulation and the numerical technique used. In Sec. IV we will give detailed simulation results. We will determine the type of every MHD discontinuity present in the flow.

Section V contains a discussion of our results. In Sec. V A we will explain why a traditional concave-inward bow shock geometry (Fig. 1a) is not possible in the switch-on regime. We will make use of the Steinolfson and Hundhausen[9,10] analysis of the symmetry of flows in the switch-on regime. Our results show very clearly the presence of intermediate shocks. These types of discontinuities were considered unphysical for a long time.[12,13] Recent numerical and analytical study shows that intermediate shocks can be physical,[14–21] and we will try to relate our results to these recent developments. The MHD flux function is nonconvex,[22,20,21] and we will try to identify intermediate shocks of the ''sonic'' type—which are a manifestation of the nonconvexity of the MHD equations—in our simulation results. This will be discussed in Sec. V B. We will conclude in Sec. VI.

II. MHD DISCONTINUITIES

In anticipation of the occurrence of MHD discontinuities of all types in the simulation results we wish to present, it is useful to give a brief introduction of MHD discontinuities[12,13,8] and an explanation of the nomenclature and notation we will use further on in this paper.

The equations of ideal one-fluid MHD in conservative form are given by

$$\frac{\partial}{\partial t}\begin{bmatrix}\rho\\ \rho\mathbf{v}\\ \mathbf{B}\\ e\end{bmatrix}+\nabla\cdot\begin{bmatrix}\rho\mathbf{v}\\ \rho\mathbf{v}\mathbf{v}+I(p+\mathbf{B}\cdot\mathbf{B}/2)-\mathbf{B}\mathbf{B}\\ \mathbf{v}\mathbf{B}-\mathbf{B}\mathbf{v}\\ (e+p+\mathbf{B}\cdot\mathbf{B}/2)\mathbf{v}-(\mathbf{v}\cdot\mathbf{B})\mathbf{B}\end{bmatrix}=0. \tag{1}$$

Here ρ and p are the plasma density and pressure, respectively, $\mathbf{v}$ is the plasma velocity, $\mathbf{B}$ the magnetic field and

$$e=\frac{p}{\gamma-1}+\rho\frac{\mathbf{v}\cdot\mathbf{v}}{2}+\frac{\mathbf{B}\cdot\mathbf{B}}{2} \tag{2}$$

is the total energy density of the plasma. I is the unity matrix. The magnetic permeability $\mu=1$ in our units. We take $\gamma=5/3$ for the adiabatic index.

MHD allows for 3 linear wave modes, the fast, the Alfvén and the slow wave, with (positive) anisotropic wave speeds satisfying $c_f \geqslant c_A \geqslant c_s$ in standard notation. The MHD Rankine–Hugoniot relations, relating the jumps across a discontinuity with the propagation speed of the discontinuity, can readily be derived.[12,13,8,23] A general property of MHD discontinuities is that the normal magnetic field component B_x is continuous (in this section we choose the x and the y coordinates normal and parallel to the surface of discontinuity, respectively). MHD discontinuities can be divided in three classes. For shocks there is both a mass flow through the surface of discontinuity, and an increase in the quantity $s=p/\rho^\gamma$ (which we will call the entropy). For contact and tangential discontinuities, there is an entropy jump, but no mass flow. For rotational discontinuities, there is a mass flow, but no entropy change.

A. Shocks

Generally up to four plasma states can be found that satisfy given values for the fluxes of mass, momentum and energy through the discontinuity surface, with the possibility that a pair of those states can be connected by a shock. These states are conventionally labeled states 1, 2, 3 and 4, ordered by increasing entropy (Fig. 3). State 1 has the lowest entropy, and in a frame moving with the shock the normal plasma velocity $v_x^{(1)}$ is larger than the normal fast MHD wave speed, so that the flow is superfast (and, therefore, also super-Alfvénic and superslow). This means that the normal fast Mach number $M_f^{(1)}$ (normal plasma velocity divided by normal fast MHD wave speed) is greater than one (the same for the Alfvén and slow Mach number). State 2 is subfast, but super-Alfvénic and superslow. State 3 is subfast and sub-Alfvénic, but superslow. State 4 is subfast, sub-Alfvénic, and subslow. In a frame of reference that moves with the shock, a particle that moves from the upstream region (traditionally indicated as region 1) to the downstream region (region 2), necessarily has to undergo an increase in entropy. So 1–2, 1–3, 1–4, 2–3, 2–4, and 3–4 are the possible entropy-satisfying shock transitions. In Fig. 4 we summarize some of their properties.

Transition 1–2 is called a fast shock (Fig. 4a). The plasma is superfast upstream and subfast (but super-Alfvénic) downstream. A fast shock increases B_y (because p is in phase with $\mathbf{B}$ for a fast wave), such that magnetic field lines are refracted away from the shock normal. Transition 3–4 is called a slow shock (Fig. 4b). The plasma is superslow (but sub-Alfvénic) upstream, and subslow downstream. A slow shock decreases B_y (because p is in anti-phase with $\mathbf{B}$ for a slow wave), such that magnetic field lines are refracted towards the shock normal. Transitions 1–3, 1–4, 2–3 and 2–4 are called intermediate shocks (Fig. 4c). The plasma is super-Alfvénic upstream, and sub-Alfvénic downstream. An intermediate shock changes the sign of B_y, such that magnetic field lines are flipped over the shock normal.

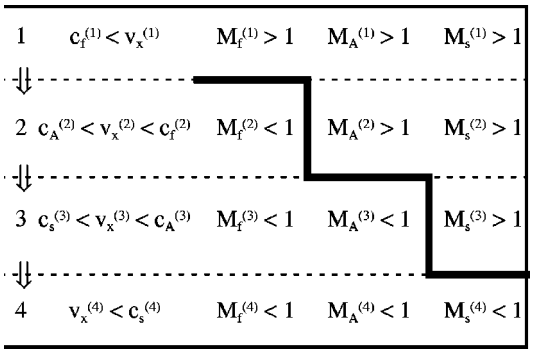

FIG. 3. Possible states that can be connected through a MHD shock. They are ordered by increasing entropy, with the lowest entropy for state 1. The normal fast, Alfvén and slow wave speeds are c_f, c_A and c_s, respectively. The normal plasma speed is v_x. The fast, Alfvén and slow normal Mach numbers are M_f, M_A and M_s, respectively. State 1 is superfast, because its normal velocity in the shock frame is larger than the normal fast MHD wave speed. Therefore the fast, Alfvénic and slow Mach numbers are all greater than one. State 2 is subfast but super-Alfvénic. State 3 is sub-Alfvénic but superslow. State 4 is subslow. Possible shock transitions are 1–2 (fast), 3–4 (slow) and 1–3, 1–4, 2–3, 2–4 (intermediate).

There exist limiting cases of these types of shocks. A fast 1–2=3 switch-on shock (Fig. 4d) has $B_{y,1}=0$ upstream. The downstream $B_{y,2}$, however, does not vanish. The tangential component of the magnetic field is thus switched on, hence the name of this shock. The angle θ is nonvanishing only if the upstream normal velocity component lies in the switch-on region between the upstream normal Alfvén speed and a critical velocity defined by

$$c_{A,1}<v_{x,1}<c_{A,1}\sqrt{\frac{\gamma(1-\beta)+1}{\gamma-1}}=v_{crit}, \tag{3}$$

with $\beta=2p/B^2$ the plasma β. Switch-on shocks can thus only exist when $\beta<2/\gamma$ (or the normal Alfvén speed $c_A>\sqrt{\gamma p/\rho}$). For a fast switch-on shock, the downstream normal Alfvénic Mach number is exactly equal to one. A slow 2=3–4 switch-off shock (Fig. 4e) has $B_{y,2}=0$ downstream. The upstream $B_{y,1}$, however, does not vanish. The tangential component of the magnetic field is thus switched off, hence the name of this shock. For a slow switch-off shock, the upstream normal Alfvénic Mach number is exactly equal to one. A limiting case of intermediate shocks are shocks that do not change the magnetic field, and those shocks are called 1–4 hydrodynamic (or parallel) shocks (Fig. 4f). Both $B_{y,1}$ and $B_{y,2}$ are equal to zero.

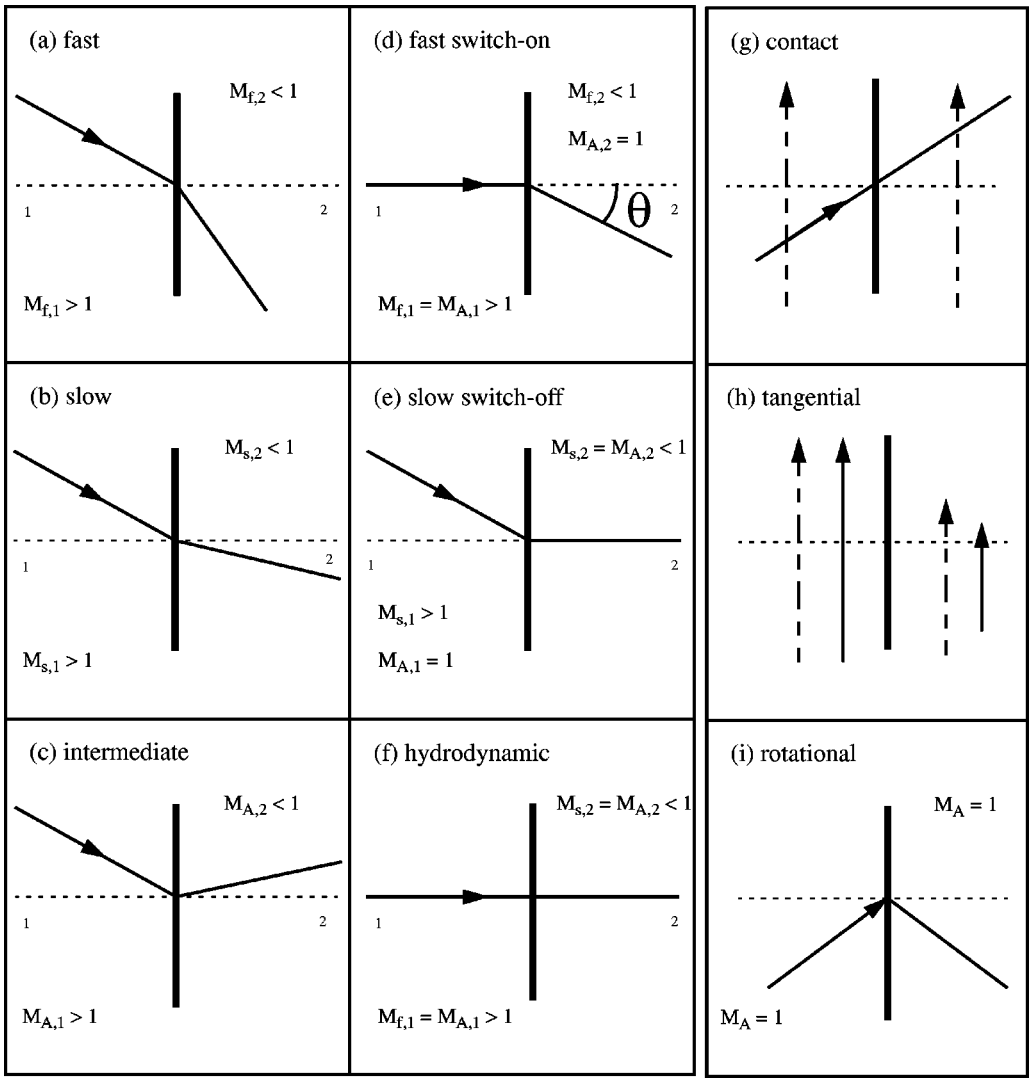

FIG. 4. Some properties of MHD shocks and discontinuities. The thick vertical line is the shock surface. The shock normal is dotted. The full arrowed lines are magnetic field lines that are refracted through the shock surface. The dashed arrowed lines are velocity vectors. Region 1 is upstream, 2 is downstream.

B. Other discontinuities

Contact discontinuities (Fig. 4g), with vanishing v_x but nonzero B_x, have only a jump in density (and entropy). All other quantities are continuous. Tangential discontinuities (Fig. 4h), with vanishing v_x and B_x, have a jump in density, pressure and tangential velocity and field. However, the total pressure $p+B^2/2$ is continuous. Planar rotational discontinuities (Fig. 4i) rotate the magnetic field around the normal of the discontinuity surface over an angle of 180 degrees, without a jump in entropy. The normal plasma velocity v_x equals $B_x/\rho^{1/2}$, such that the normal Alfvénic Mach number equals one on both sides.

III. SETUP OF THE NUMERICAL SIMULATION

In this section we describe the setup of the numerical simulation and we discuss the numerical technique used. We will also discuss some invariants and constraints of this problem, which will help us with the interpretation of the simulation results.

A. Setup and numerical technique

In our simulations a 2D uniform field-aligned flow in planar symmetry ($\partial/\partial z=0$) enters from the left and encounters a perfectly conducting rigid cylinder. The resulting stationary ideal MHD flow is completely determined by the inflow plasma β and the inflow Alfvénic Mach number in the direction of the flow speed. For the incoming flow we choose $\beta=0.4$, which implies a critical Alfvénic Mach number $M_{A,crit}=1.732$ [Eq. (3)]. We choose the Alfvénic Mach number of the incoming flow $M_A=1.5$, such that the parameter regime of our simulation allows for switch-on shocks. The x axis being horizontal, we can choose $\rho=1$ and $B_x=1$ (implying that the Alfvén speed along the field lines $c_A=1$). The pressure and velocity can then be determined from β and M_A, yielding $p=0.2$ and $v_x=1.5$ (such that the acoustic Mach number $M=1.5\sqrt{3}$). Finally, we take $B_y=0$ and $v_y=0$. As the resulting stationary ideal MHD flow will be scale invariant, we can freely choose the radius of the cylinder. We take $r=0.125$ and the cylinder is placed at the origin of the coordinate system. We simulate the flow in the

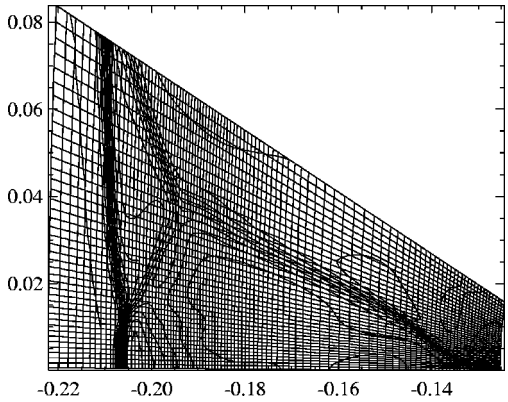

FIG. 5. Detail of the stretched structured simulation grid. The cylinder is not shown, but is located to the right. We show density contours of the converged solution. The shocks are generally well resolved.

upper left quadrant, on a 120×120 stretched elliptic polar-like structured grid, extending to $x=-0.35$ on the x axis, and to $y=1.4$ on the y axis. Part of the simulation grid is shown in Fig. 5. We impose the above described uniform flow as the initial condition. We use ghost cells to specify the boundary conditions. On the left, we impose the uniform superfast incoming flow. The cylinder wall is an ideally conducting wall. We look for a stationary flow solution with top–bottom symmetry,[9,10] such that the horizontal line which extends to the center of the cylinder is the stagnation line, parallel to the incoming flow (Fig. 1). This stagnation line, which is a streamline and a magnetic field line, then has the same symmetries as an ideally conducting wall. This symmetry has to be imposed in the boundary condition on the lower border of the simulation domain in order to obtain a stationary symmetrical solution. The simulated bow shock flow in the upper quadrant can thus also be thought of as a 2D model flow over a perfectly conducting plate (the stagnation line) with a semi-circular bump or corner. The right outflow condition is superfast, so there we extrapolate all quantities to the ghost cells. The flow evolves in time until a converged steady state bow shock solution is obtained.

We solve Eq. (1) using a conservative finite volume high resolution Godunov shock capturing scheme which is second order in space and time, employing a slope-limiter approach[24,5,7] with minmod-limiting on the slopes of the primitive variables. The time-integration is explicit with a two-step Runge–Kutta method. This code was extensively tested and the test results were compared with results from other codes. The code was previously used for resistive MHD simulations of interacting hot filaments in a tokamak.[25]

For our present simulations, we use the Lax–Friedrichs numerical flux function,[24,26,27] which is simple and robust. Contact and tangential discontinuities are not perfectly well resolved due to the relatively high numerical dissipation for these waves, but shocks are well resolved in a steady state calculation. We did not use Roe's scheme[28] although this scheme in theory could resolve shocks and, especially, tangential discontinuities much better. We have found several problems while trying to apply this scheme to our simulation. Roe's scheme suffers from various instabilities, like the carbuncle-instability,[29] and in consequence of these instabilities, a steady state solution could not be obtained with this scheme. Using the Lax–Friedrichs scheme, we obtained convergence of more than eight orders of magnitude in the norm of the density residual.

We carefully checked if the results we obtained do not contain numerical artifacts or features dependent on the numerical resistivity. We did many simulations with grids of different cell sizes and we obtained uniform grid convergence to the solution shown in Fig. 2. We also did simulations on uniform grids and grids with a different accumulation of points than in the grid of Fig. 5, and refinement studies using these different grids resulted in grid convergence to the same solution of Fig. 2. The fully consistent and complete physical interpretation of all the features in the solution to be presented in the next section, gives further confidence that the features present in our solution are real and physically meaningful.

We use a projection scheme[30,26] to keep the $\nabla\cdot\mathbf{B}=0$ constraint satisfied. After every time step a small correction is added to the magnetic field, resulting in a solution scheme that guarantees $\nabla\cdot\mathbf{B}=0$ up to machine accuracy in the chosen discretization.

B. Invariants and constraints

The problem considered in this paper has several interesting invariants and constraints,[1] which we can use for the interpretation of the results and the performance assessment of the numerical method. The solution is in a steady state, meaning that fluid element paths are stationary curves, called streamlines. For a smooth flow, the entropy remains constant for a fluid element, so the streamlines have to coincide with entropy contours. At shocks, however, the entropy increases. If $\mathbf{v}\|\mathbf{B}$ in the inflow (meaning that the electric field is zero), then this property will be conserved throughout the whole flow, also through shocks. If $\mathbf{v}\|\mathbf{B}$ everywhere, then the stagnation enthalpy,

$$h_s=\frac{\gamma p}{(\gamma-1)\rho}+\frac{v^2}{2}, \tag{4}$$

is constant on streamlines, also across shocks. As the incoming flow is uniform, the stagnation enthalpy should remain constant over the whole simulation domain. If $\mathbf{v}\|\mathbf{B}$ everywhere, then the normal Alfvénic Mach number becomes independent of the direction:

$$M_A(\theta)=\frac{v(\theta)}{B(\theta)/\sqrt{\rho}}=\frac{v}{B/\sqrt{\rho}}. \tag{5}$$

This means that the Alfvénic Mach number is isotropic and can easily be determined and plotted, greatly facilitating the determination of MHD shock types. The RH relations for the shock on the stagnation streamline are simple and can be solved easily,[1] resulting in downstream quantities $p=1.64$, $\rho=2.77$, $v_x=0.542$ and $s=0.300$. In the next section we will show that the numerical solution reproduces these quantities.

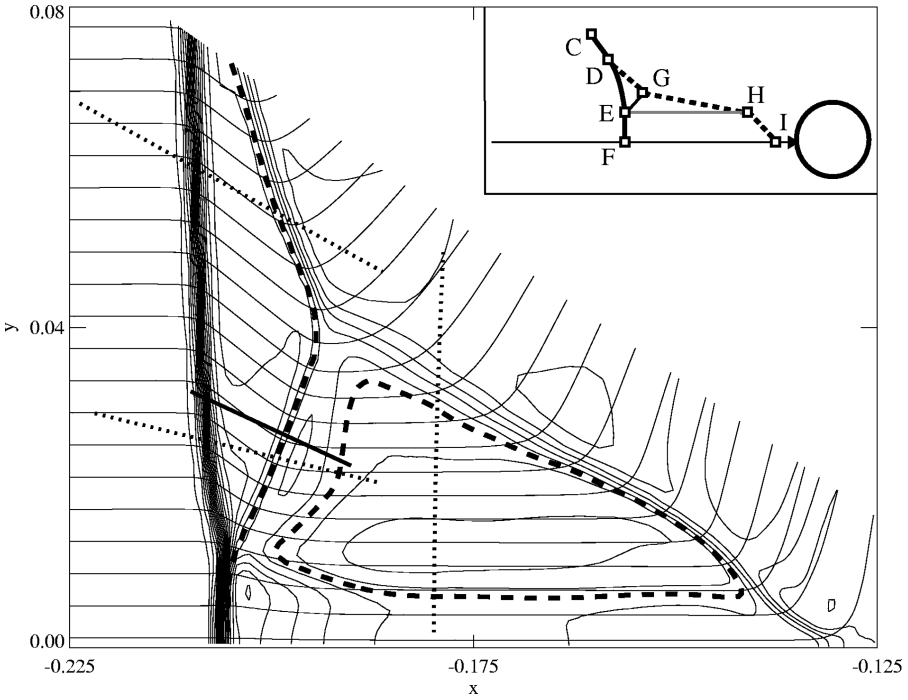

FIG. 6. Detail of the solution in the half plane above the stagnation streamline. We show Alfvénic Mach number contours (piling up in the shocks) and magnetic field lines (coming in horizontally on the left). The dashed line is a contour where the Alfvénic Mach number exactly equals one. This information together with the refraction of the field lines serves to identify the shocks as fast, hydrodynamic and intermediate (see the text).

As **v** and **B** are both constrained to lie in the *xy* plane, linear Alfvén waves oscillating out of the *xy* plane as a separate fundamental mode, can not be present in the simulated flow. However, intermediate shocks can in principle be present, because of the highly nonlinear interactions in the flow with shocks.

IV. INTERPRETATION OF THE SIMULATION RESULTS

In this section we will show our simulation results in detail. We will show how the type of all arising MHD discontinuities can be clearly determined. For the identification of shock parts we refer to the lettering labels of Fig. 1c.

In Fig. 2 we show a global view of the converged bow shock solution. The uniform flow comes in from the left. We clearly see the dimple in the central part of the shock front, confirming this particular aspect of the Steinolfson and Hundhausen[9] analysis. However, behind the leading shock front, we see a rich structure of several other shocks with intricate field line refractions. The leading shock front (composed of fast and intermediate shocks) is followed by a second shock front. The refraction of the field lines (away from the shock normal) above point B of Fig. 1c shows that this part of the shock front is a fast shock.

In Fig. 6 we show a detail of the flow in the half plane above the stagnation streamline. D–E is a fast shock with $B_{y,1}$ almost vanishing upstream, so it is almost a fast switch-on shock. E–F is a 1–4 hydrodynamic intermediate shock. (It could be slightly concave-inward and thus not of the hydrodynamic type at locations on the front away from point F, but this is hard to tell at the resolution of our simulations. At point F, the shock is definitely of the hydrodynamic type.) E–G is an intermediate shock, because it clearly contains the dashed $M_A=1$ contour (showing that the flow goes from super-Alfvénic to sub-Alfvénic upon passing through the shock), and because the field lines are flipped over the normal. In Sec. V B it will be shown that shock E–G is a 1=2–3=4 intermediate shock. D–G–H–I is an intermediate shock with an upstream Alfvénic Mach number (slightly) greater than one, and with magnetic field lines that are flipped over the normal. At various places along the shock front, the upstream intermediate Mach number approaches one and the downstream magnetic field becomes almost normal to the front, meaning that the shock is close to a 2=3–4 slow switch-off shock at those places. The intermediate shock is thus of the 2–4 type, close to a 2=3–4 slow switch-off shock. E–H is a tangential discontinuity. Other tangential discontinuities are stretching out from points D, G and H along the streamlines to infinity. E–F is very reminiscent of a Mach stem as it occurs in Hydrodynamic shock reflection.[31] *A priori* the point E could lie on the stagnation streamline, in which case this point would be a singular point on this streamline where four shock branches interact. In such a situation, the stagnation streamline would not be a shock normal. In such a hypothetical singular point, the $\nabla\cdot\mathbf{B}=0$ constraint could be satisfied if the jump in B_y in the *y* direction is exactly the same (with opposite sign) as the jump in B_x in the *x* direction. A solution with such a singular point is found for the simulation on a grid with low spatial resolution. With sufficient resolution, however, the shock part E–F appears, reducing the singularity to three branches interacting in point E. An interaction point where four branches meet seems thus to be avoided. This may be a more general feature of MHD shock interaction, at least for some types of shocks.

In Fig. 7 we show a detail of the region close to the ''nose'' point B. The shock at point B is a 1–2=3 fast switch-on shock, because the tangential field component is switched on, and because the downstream Alfvénic Mach number equals one. B–C–D is an intermediate shock, be-

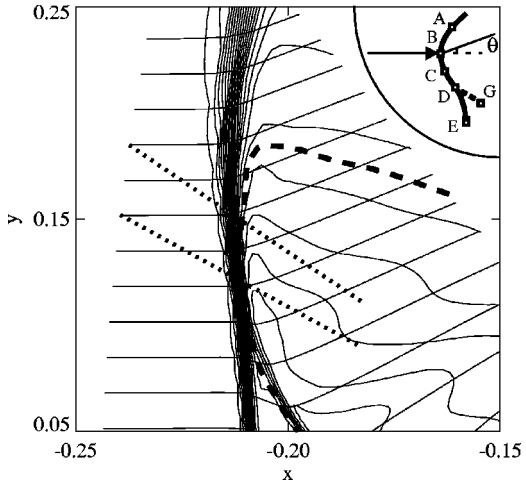

FIG. 7. Detail of the solution close to the ''nose.'' We show Alfvénic Mach number contours and magnetic field lines. The dashed line is a contour where the Alfvénic Mach number exactly equals one. This information together with the refraction of the field lines serves to identify the shocks as fast and intermediate (see the text).

cause it clearly contains the dashed $M_A=1$ contour, and because the field lines are flipped over the normal. Shock B–C–D is of the 1–3 type, which can be merged continuously with the fast 1–2=3 switch-on shock in point B.

In Fig. 8 we show plots of the variables along the stagnation streamline. The first feature we encounter when we go from left to right is a discontinuity which corresponds to the hydrodynamic shock at point F. The jumps of the density, pressure, velocity and entropy agree well with the jumps calculated from the RH relations in Sec. III B. The fast, Alfvénic, and slow Mach number all jump from above one to under one, indicating a 1–4 intermediate shock. The magnetic field does not show a jump consistent with a purely hydrodynamic shock.

Going further to the right, we see that we pass through a rarefaction to reach a constant state. This slow rarefaction converges the flow slightly towards the stagnation streamline. Although the flow near the stagnation line may appear to be close to a 1D flow in Fig. 6, the flow is, in fact, 2D at various places along the stagnation line. In Fig. 8d we plot $\partial B_y/\partial y$ (thin line), indicating that the flow is 2D in this rarefaction region. The density decreases in the main direction of the converging flow on the stagnation line, because the velocity (v_x) is increasing and $\nabla\cdot(\rho\mathbf{v})=0$. B_x is not significantly influenced by the increasing v_x because the field is aligned to the flow. However, B_x increases along the flow because of the 2D effect of converging flow in the y direction perpendicular to the stagnation line. This flow component causes the field lines to converge towards the stagnation line, as can be seen in Fig. 8d: $\partial B_x/\partial x$ balances $\partial B_y/\partial y$ such that $\nabla\cdot\mathbf{B}=0$.

Going further to the right, we pass a region where the flow is uniform. The flow becomes 2D again as we approach the stagnation point at the cylinder, as can be seen in Fig. 8d. This is no surprise, because, in general, every stationary stagnation point flow is necessarily 2D due to the requirement of mass conservation [$\nabla\cdot(\rho\mathbf{v})=0$]. Indeed, a stagnation point can clearly not be reached by means of a stationary 1D flow (neither a shock nor a continuous flow), because a 1D flow can not bring ρv_x down from a finite value to a value of zero at the stagnation point.

As a clear example of a stationary 2D stagnation point flow, we show in Fig. 9 how a stagnation point is reached in a traditional single-front MHD bow shock flow, which is obtained by choosing the inflow velocity outside of the switch-on region [Eq. (3)]: $\rho=1$, $p=0.2$, $v_x=2$, $v_y=0$, $B_x=1$, and $B_y=0$ at the inflow, resulting in inflow Mach numbers $M_A=2$ and $M=2\sqrt{3}$ ($\beta=0.4$). The stagnation point is reached in a continuous (constant-entropy) 2D compressive

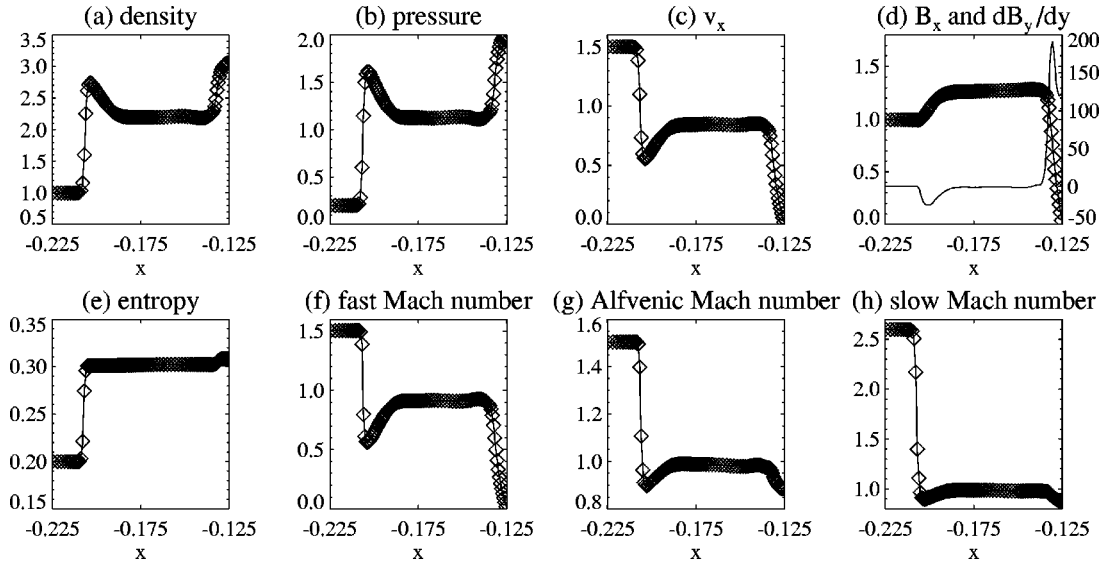

FIG. 8. Plots of the variables along the stagnation streamline. From left to right, the uniform incoming flow first jumps in the hydrodynamic shock, followed by a slow rarefaction, which brings the flow back to uniform. Close to the cylinder we pass the intermediate shock. The flow is then brought to the stagnation point in a continuous diverging compression. The variation of $\partial B_y/\partial y$ in (d) (thin line, axis on the right) shows that the flow is effectively 2D at various locations on the stagnation line.

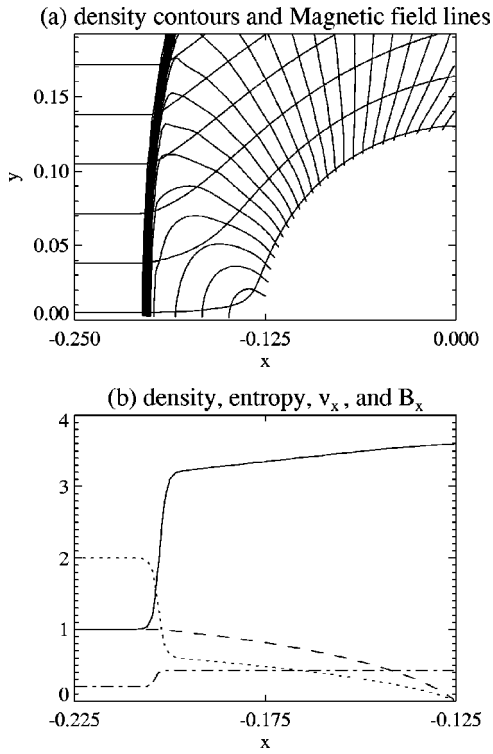

FIG. 9. Simulation of a MHD flow with a single-front bow shock (inflow Mach numbers $M_A=2$ and $M=2\sqrt{3}$, and $\beta=0.4$). (a) Flow near the cylinder. (b) Stagnation line variables. Behind the shock, the flow variables are brought to their stagnation point values in a continuous compressive diverging flow. B_x is dashed, v_x dotted, s dash–dotted and ρ full.

diverging flow region behind the shock front.

In our simulation, the 2D stagnation point flow is complicated by the presence of intermediate shock D–G–H–I. Figure 2 shows that point I lies very close to the cylinder. In this region very close to the cylinder we expect the 2D stagnation point flow. Because this region is extremely small compared to the dimensions of the other features in our simulation, we have a comparatively low numerical resolution in this region. Moreover, the curvature of the intermediate shock front at point I is very large and may even be singular, which makes the post-shock flow 2D and complicates the interpretation of the shock as a 1D shock.

All these complications make the interpretation of the simulation results near the cylinder quite difficult. However, we can propose the following possible interpretation for the variation of the flow variables near the cylinder in Fig. 8.

The location of the small jump in entropy in Fig. 8e close to the cylinder can reasonably be identified with the point I of Fig. 6, where the intermediate shock D–G–H–I intersects the stagnation line. This entropy jump is located at a finite distance from the cylinder, which means that there is a small but finite standoff distance between the shock and the cylinder. In the small constant-entropy region between point I and the cylinder, we can expect a continuous 2D stagnation point flow analogous to the flow in Fig. 9. The variation of ρ, v_x and B_x close to the cylinder in Fig. 8 appears to be consistent with the continuous variation of these quantities in the stagnation point flow of Fig. 9.

Although not conclusively proven, this interpretation of the flow near the cylinder in Fig. 8 as a weak shock followed by a 2D compressive diverging stagnation point flow is reasonable because it is consistent with the simulation data and because it establishes a clear analogy with less complicated stagnation point flows. It will be interesting to see if future simulations with more powerful numerical techniques will confirm all the details of this interpretation of the highly complicated stagnation point flow.

In Fig. 10 we show plots of some variables along several instructive 1D cuts. Figures 10a–c show a cut along the lower dotted line cutting the leading front in Fig. 6 under an angle of $\theta=13.82$ degrees. The dotted line is a part of a ray through the center of the cylinder. First we cross the fast shock. Then the intermediate shock brings the Alfvénic Mach number from above one to under one. Figures 10d–f show a cut along the upper dotted line cutting the leading front in Fig. 6 ($\theta=29.25$). Again we cross the fast shock first. Then we cross the intermediate shock, with the upstream Alfvénic Mach number close to one. Figures 10g–i show a cut along the lower dotted line cutting the leading front in Fig. 7 ($\theta=47.66$). We cross only one shock, which is of the intermediate type, because it brings the Alfvénic Mach number from above one to under one. Figures 10j–l show a cut along the upper dotted line cutting the leading front in Fig. 7 ($\theta=53.40$). We cross the same intermediate shock.

In Fig. 11 we show plots of some variables along the vertical dotted line in Fig. 6. Where the pressure jumps for the first time, we pass through the tangential discontinuity (a little more smeared out than the shocks), as is proved by the continuity of the total pressure here. The next jump is the intermediate shock, with an upstream Alfvénic Mach number close to one. (This profile is a little smeared out because we cross it under a large angle).

V. DISCUSSION

In this section we will discuss how topological constraints lead inevitably to the complicated solution for a bow shock flow in the switch-on regime that we have found in our simulation results. We will then discuss the presence of intermediate shocks in our simulation results and investigate if some of the shocks present in our simulation results can be related to the nonconvexity of the MHD equations.

A. Topological problem for a concave-inward bow shock

In this section we discuss the topological problem of a concave-inward shock solution for a flow in the switch-on regime, along the lines of the ideas of Steinolfson and Hundhausen.[9,10]

Suppose a uniform field-aligned magnetized flow with a flow velocity lying in the switch-on region [Eq. (3)] is obstructed by a perfectly conducting cylinder. A bow shock will result. If the magnetic field were absent, a hydrodynamic bow shock would have the classical well-known concave-inward (to the cylinder) geometrical shape (Fig. 1a). For a MHD bow shock in the switch-on regime, such a geometry is physically not admissible. Because of symmetry, the mag-

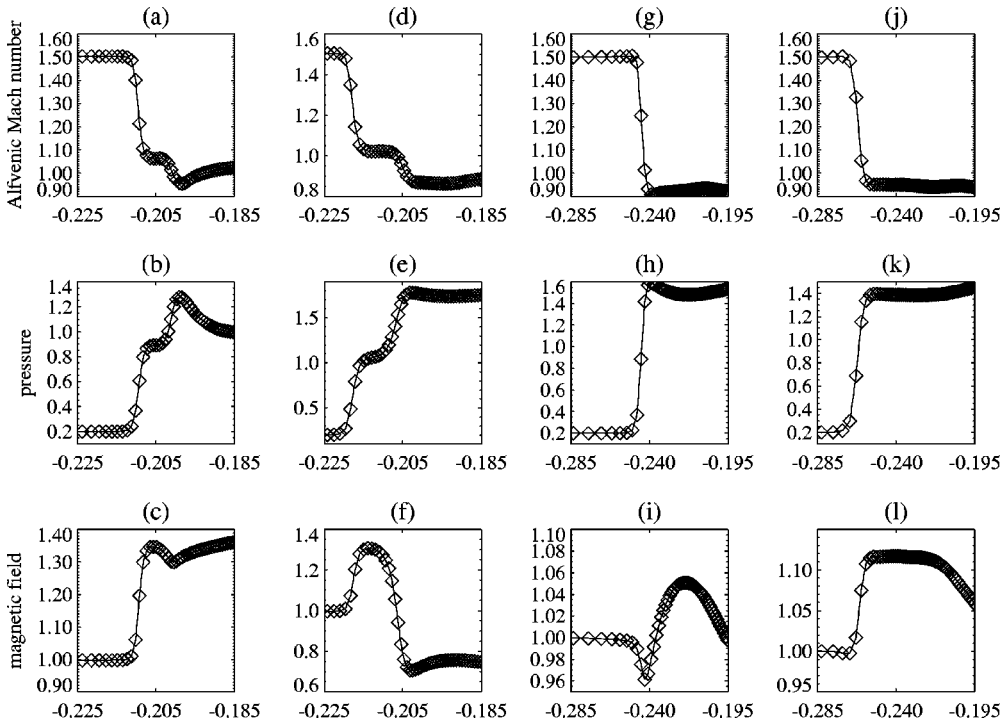

FIG. 10. Alfvénic Mach number (a), (d), (g), (j), pressure (b), (e), (h), (k) and magnetic field (c), (f), (i), (l) along various cuts through the simulation domain. (a)–(c) Cut along the lower dotted line cutting the leading front in Fig. 6. (The lower axis shows the distance to the center of the cylinder.) We pass the fast shock, and then the intermediate shock followed by a rarefaction. (d)–(f) Cut along the upper dotted line cutting the leading front in Fig. 6. We pass the fast shock, and then the intermediate shock. (g)–(i) Cut along the lower dotted line cutting the leading front in Fig. 7. We cross the intermediate shock. (j)–(l) Cut along the upper dotted line cutting the leading front in Fig. 7. We cross the intermediate shock.

netic field line which coincides with the stagnation streamline [stretching horizontally from infinity to the stagnation point ($\mathbf{v}=0$) at the cylinder; line F–I in Fig. 1c] has to be a straight line. In other words, on this line, the field is not deflected by the shock. At the point where a shock front crosses this line, the shock is necessarily of the hydrodynamic type. Away from this point along the shock front, the shock has to be a fast MHD shock, with the field refracted away from the normal (Figs. 1a and 4a) in order to have the post-shock flowing plasma drape around the cylinder. As we move along this fast shock front closer and closer to the intersection of the front with the stagnation line, the upstream tangential component of the magnetic field goes to zero. But when the upstream velocity lies in the switch-on region, the downstream tangential component of the magnetic field does not vanish as we approach this intersection point, resulting in a switch-on shock with a finite turning angle θ, as illustrated in Fig. 1a. Clearly, approaching the stagnation line from its two sides along the fast shock front, would lead to two switch-on shocks of opposite deflection. This means that there is a discontinuity between the two physical states on the two sides of the stagnation field line. Such a discontinuity is not physically justified, so the assumed concave-inward shock geometry needs to be modified to avoid the discontinuity.

Petrinec and Russell[1] suggest that some form of symmetry breaking could solve this problem. The symmetry could be broken by relaxing the field-aligned condition, but this requires a treatment in three dimensions (see Sec. VI). Steinolfson and Hundhausen[9] propose a solution with a different geometry for the shock front in 2D without the need to break the symmetry. They add a level of complexity by allowing for a shock front composed of segments of different MHD shock types. Based on the analysis of the RH relations

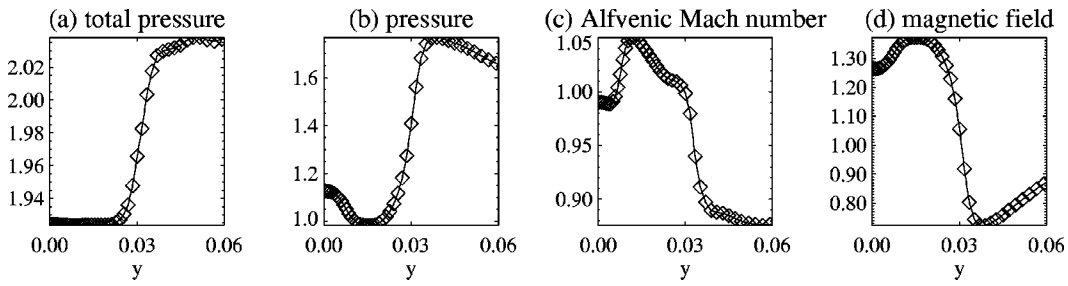

FIG. 11. The cut along the vertical dotted line in Fig. 6. We first cross the tangential discontinuity, with a jump in pressure but not in total pressure. Then we pass the intermediate shock.

along the shock front, they propose a front that is composed of fast and intermediate shocks, with physical parameters continuously varying along the front (Fig. 1b). In such a topology, the central part of the front has a concave-outward (''dimpled'') geometry and is composed of two types of intermediate shocks (1–3 and 1–4). The 1–4 shock can continuously be linked to the hydrodynamic shock at the stagnation line. The 1–3 shock can be linked continuously to the switch-on shock at the new ''nose'' of the front. Time-dependent 2D MHD simulations[9,10] partially confirmed this picture (a dimpled shock front is formed), and dimpled fronts were also observed in coronagraph images of fast moving CMEs.[9–11] However, Steinolfson and Hundhausen point out that there remain some problems with this shock topology. The 1–3 and the 1–4 shock can only be continuously linked under one specific angle (given the inflow conditions). This angle would, for instance, be independent of the shape of the object. This seems to imply that this solution does not take into account the specific downstream flow. This is not really a surprise, because the analysis is only based on the 1D RH relations along the front. Their time-dependent 2D simulation results for a uniform upstream field did not fully confirm the shock geometry they proposed from 1D theoretical analysis. In their numerical results they found several features for which they could not provide a clear interpretation, including traces of slow shocks, an unusual ''tube'' configuration near the symmetry line and a possible singular point where four shock branches would interact.[9]

Our new simulations of the 2D steady state MHD bow shock problem in the switch-on regime were carried out with a high resolution shock capturing numerical technique. The solution is stationary in time, which greatly facilitates a clear interpretation. Our simulation results confirm aspects of the Steinolfson and Hundhausen theoretical analysis and clarify many of the unclear features present in their numerical results. We show that a steady state solution of the symmetrical bow shock problem does exist in 2D, but our solution reveals and explains much richer and more complex physics not anticipated in the important earlier work of Steinolfson and Hundhausen. Clearly an additional level of complexity is present: not only do shocks of several different types form in the leading front, but the requirement of continuously varying physical parameters along the shock front may not be met. This happens at the interaction points between shock fronts. These multiple shock fronts are necessary to channel the flow around the object.

It is conceivable that our results on shock topology in stationary flows in the switch-on regime can also be important for shock propagation in time-dependent flows in this regime. Detailed simulations of time-dependent flows in the switch-on regime will be the subject of further research.

B. Intermediate shocks and nonconvexity

There has been much controversy about the physical existence of intermediate shocks. For a long time, the belief has been accepted that intermediate shocks are unphysical.[12,13] This belief was based upon approximate analysis of 1D discontinuous solutions of the ideal equations, e.g., linear stability analysis leading to the concept of ''evolutionarity,'' geometrical conditions, nonlinear stability, etc.[20] Recently this belief has been challenged from several points of view. Intermediate shocks were encountered in 1D and 2D numerical simulations of the ideal MHD equations[22,9,10] and they were observed in space plasmas.[32] The early results on the inadmissibility of intermediate shocks thus seem not to be valid. These results were obtained in the framework of the classical theory of MHD shocks, which is a discontinuity theory based on analysis of the ideal equations.[12,13] Recently, Wu has pioneered a new approach, based on analysis of the MHD Navier–Stokes equations (see Ref. 16 for a review). In this dissipative theory, numerical and analytical investigation of the formation and physical admissibility of 1D intermediate shocks shows that intermediate shocks can be formed by wave steepening and can have viscous profiles.[14–21] Nonplanar problems in dissipative MHD lead to the phenomenon of time-dependent intermediate shocks.[14,33,34] Intermediate shocks described by a scalar nonconvex equation exhibit MHD-like behavior, and their admissibility depends on the ratio of dissipative and dispersive coefficients.[16] It was suggested by Wu that the dissipation mechanism for shock waves has to be taken into account for any system which possesses more than two stationary points for its shock structure equations and whose shock structure solutions depend on the dissipation mechanism.[16] Since the evolution of intermediate shocks in a dissipative theory may depend on the shock structure, hybrid and kinetic approaches[35] do not always give results consistent with MHD findings.

Most theoretical analysis is done for 1D discontinuities. Recent theoretical work on translation symmetric stationary 2D MHD flows[23] describes explicit self-similar solutions for such flows with fast, intermediate and slow shocks.

Also, most of the new theoretical results on intermediate shocks have only been confirmed in 1D numerical simulations. Intermediate shocks of the 1–3, 1–4, 2–4 and 1=2–3=4 types are clearly identified in our steady state 2D simulation results. Based on an analysis of the dissipative equations in 1D, it has been shown recently that all of these shocks can have viscous profiles in the planar MHD case.[14–21] Our simulation results are thus the first clear confirmation in two space dimensions of many aspects of the new theoretical results on intermediate shocks.

The Steinolfson and Hundhausen analysis is very interesting from the perspective of the issue of the physical existence of intermediate MHD shocks. It follows from their analysis of the topology of a planar 2D MHD flow configuration that intermediate shocks are necessary ingredients of certain 2D MHD flows. Their analysis was incomplete and our results show that the flow pattern can be more complex than they anticipated, but our simulation results confirm that intermediate shocks are indeed needed to drape a field-aligned flow around an object in certain parameter regimes. In 1D Riemann problems, it could always be argued that field rotations can be performed by rotational discontinuities, and that intermediate shocks are thus unnecessary. But in driven 2D problems, once the 1D degeneracy has been removed, the situation seems different. In the flow under con-

sideration, just under the ''nose'' of the shock front (for example, point B in Fig. 1c), intermediate shocks seem to be topologically inevitable. The hydrodynamic shock on the stagnation streamline has necessarily to be a 1–4 intermediate shock.[17] These geometrical considerations based on planar 2D flow configurations seem to be an independent indication that MHD intermediate shocks have to exist and naturally arise in realistic initial value problems, as confirmed by our simulations. It is very hard to prove rigorously that a solution with only rotational discontinuities and without intermediate shocks does not exist for the 2D flow problem discussed in this paper. But the above arguments, mainly of a heuristic nature, seem to show that the existence of a solution without intermediate shocks is unlikely, and that intermediate shocks appear naturally.

A scalar nonlinear conservation law is described by

$$\frac{\partial u}{\partial t}+\frac{\partial f(u)}{\partial x}=0, \tag{6}$$

where $f(u)$ is called the flux function, and $\lambda=f'(u)=dx/dt$ gives the slope of the characteristics (the characteristic speed) in the xt plane. Equation (6) allows for discontinuous solutions (shocks) that propagate with a speed s determined by the RH relation

$$s=\frac{f(u_r)-f(u_l)}{u_r-u_l}, \tag{7}$$

where u_r and u_l are the states on the right and the left of the discontinuity.[24] If $f(u)$ is a strictly convex function [meaning that $f'(u)$ is strictly monotonous, or that $f''(u)$ does not vanish anywhere], then $s\in]f'(u_l),\ f'(u_r)[$. However, if $f(u)$ is not convex, then there exist states u_l and u_r such that the shock connecting u_l with u_r has a speed equal to the characteristic speed in the left or the right state, for instance, $s=f'(u_r)=\lambda_r$, or $s=\lambda_r=0$ in the shock frame. We will call such a shock a sonic shock.

The fast and the slow MHD characteristic fields are not convex.[22] So there exist 1=2–3 shocks, for which $v=c_f$ (in the shock frame) upstream, meaning that $\lambda_f=v-c_f=0=s$. Another type of sonic shock in MHD is the 2–3=4 shock, for which $v=c_s$ downstream, meaning that $\lambda_s=v-c_s=0=s$. Notice that the term 'sonic' is used here in a generic sense, denoting the condition that the plasma speed equals any of the MHD characteristic speeds.[23]

The fact that the flow is sonic upstream or downstream of the shock, allows for continuous attachment of a simple wave[31] rarefaction of the slow or fast family, moving with the same speed as the shock at the point of attachment. This structure of a sonic shock with an attached simple wave rarefaction is called a compound wave.[22,24,20] The above analysis and the definition of a compound wave remain valid in a dissipative context, because even in a dissipative theory, shocks that do not depend on time and have a finite extent, have to satisfy the ideal RH relations. Compound waves naturally arise in the solution of Riemann problems of nonconvex systems in the framework of a discontinuity theory.[24] For MHD, they were first observed in the numerical solution of planar 1D MHD Riemann problems.[22]

However, the admissibility of the intermediate shocks encountered in compound waves was questionable.[22] Both for the scalar[16] and the MHD case, the above analysis—based on the nonconvexity of the ideal flux function—is incomplete and has to be supplemented with an admissibility study using the dissipative equations.[14–21] Analysis in the dissipative framework shows clearly when sonic shocks are admissible and when they occur with attached rarefactions in solutions of Riemann problems.[15,16] Such analysis also shows that compound waves are just one of the many possible wave combinations that may appear in the solution of Riemann problems,[15,16] when they are analyzed in the appropriate dissipative context, especially for nonplanar conditions, and depending on the dissipation mechanism. Compound waves thus play a less central role than one would conclude from a discontinuity theory. The combination of a sonic shock with an attached simple wave rarefaction in a compound wave is, however, not uncommon in a planar situation, as compound waves are admissible wave combinations present in the Myong and Roe[20,21] analytical solution of some planar MHD Riemann problems. For the planar case which they treat, Myong and Roe relate the occurrence of compound waves to the inadmissibility of 2–3 undercompressive intermediate shocks, for which the compound waves—with embedded sonic intermediate shocks—are substitutes.[20,21]

It is thus interesting to look for the presence of 1=2–3 and 2–3=4 sonic intermediate shocks in our 2D simulation results, as they are a manifestation of the nonconvex nature of the equations, and to study the rarefactions that may be attached to them.

Let us first consider the hydrodynamic intermediate shock on the stagnation streamline. It is followed by a slow rarefaction (Figs. 8), but Figs. 8f–h show clearly that the flow is not sonic where the rarefaction is attached to the shock. This shock is thus not of the sonic type, and in this example, the rarefaction is a 2D effect, as noted before. It serves to bring the Alfvénic Mach number from its downstream value lower than one to a value close to one, necessary for the shock at point I.

Intermediate shock C-D (Figs. 10h–i) is followed by a rarefaction, contrary to intermediate shock B–C (Figs. 10k–l; the different behavior of the post-shock magnetic field is striking). Shock D–G–H–I seems to be followed by a rarefaction as well (Figs. 10e–f and Fig. 11d). For all of these structures, the flow is, however, not sonic where the rarefaction is attached to the shock.

Finally intermediate shock E–G remains to be investigated. This shock is followed by a clear rarefaction and preceded by another (weak) rarefaction (Figs. 10b–c and Fig. 12a). A detailed analysis of the speeds along the solid line normal to shock E–G in Fig. 6 learns that the intermediate shock is a 1=2–3=4 shock, as the downstream normal slow Mach number and the upstream normal fast Mach number are both equal to one (Figs. 12b–c). The flow is thus sonic on both sides of the shock. This is a clear manifestation of the nonconvexity of the MHD equations in a steady state 2D flow. It has been shown recently by Myong and Roe[20,21] that this type of 1=2–3=4 shock is admissible and can be

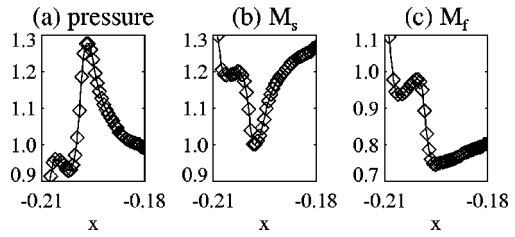

FIG. 12. The cut along the solid line normal to the intermediate shock E–G in Fig. 6. The intermediate shock is preceded and followed by rarefaction regions. The normal fast Mach number equals one where the upstream (left) rarefaction is attached to the shock. The normal slow Mach number equals one where the downstream rarefaction is attached to the shock. The intermediate shock is thus a 1=2–3=4 shock.

present in the analytical solution of planar *xt* Riemann problems, embedded in a double *xt* compound wave. The stationary 2D rarefaction–shock–rarefaction structure of our simulation result could be more closely related to this double *xt* compound wave, if the steady state rarefactions are simple waves and not merely 2D effects similar to the rarefaction following the hydrodynamic shock on the stagnation line. To investigate this, it would be interesting to compare the characteristic structure of this 2D stationary structure in the *xy* plane to the characteristic structure of the double compound wave in the *xt* plane, which has simple wave rarefactions. This has to be investigated using characteristic analysis of the steady state MHD equations and remains a topic for further study.

VI. CONCLUSION

In this paper we have presented a detailed description of an illuminating example of MHD shock interaction, which may have applications in low-β space plasmas. Our results show that a highly complicated steady state solution exists for the model problem of a 2D symmetrical bow shock flow in the switch-on regime. When the flow speed of the incoming field-aligned flow lies in the switch-on region, a second shock front forms, trailing the leading fast front. The resulting bow shock solution differs in two fundamental ways from the classical picture of a bow shock (Fig. 1a). The new bow shock flow is composed of several consecutive interacting shock fronts, instead of a single bow shock front. Furthermore, segments of different MHD shock types are present in the flow, in contrast to a flow with only fast shocks. Physical parameters vary discontinuously along shock fronts where those fronts interact. These are interesting results on MHD shock interaction in a 2D flow.

This kind of flow may be present in space plasmas. However, our simulations are done for specific parameters and in the symmetrical field-aligned 2D case, so we have to investigate how general these effects are and if they will also be present in 3D situations. We have found that the flow topology is retained when we slightly change the plasma β and the Mach number of the incoming flow. If we want to break the symmetry and relax the condition on field-aligned flow by allowing for a finite angle between the incoming velocity and magnetic field, we have to consider the 3D ideal MHD problem of a stationary flow around a sphere, because in a 2D flow the magnetic flux can not be carried around a cylinder without reconnection when the flow is not field-aligned. In this case the flow will lose some of its symmetries and the stationary solution may be different, but there will still be a position on the shock surface where the upstream magnetic field is perfectly normal to the bow shock surface.[1] The switch-on singularity would apply at such a point, which may be expected to lead to shock formation effects similar to what has been described in this paper. Such 3D simulations will be the subject of further research. Preliminary results for simulations we have carried out of a field-aligned bow shock flow around a sphere in axial symmetry show that similar shock formation phenomena occur.

Our simulation results clearly confirm that planar intermediate MHD shocks can exist and naturally arise in 2D MHD bow shock flows in the switch-on regime. Intermediate shocks are essential components of a bow shock structure that channels the field-aligned flow around an obstacle. Intermediate shocks of the 1–3, 1–4, 2–4 and 1=2–3=4 types are clearly identified in our steady state 2D simulation results. Based on analysis of the dissipative equations in 1D, it has been shown recently that all of these shocks can have viscous profiles in the planar MHD case.[14–21] Our simulation results are thus the first clear confirmation in two space dimensions of many aspects of the new theoretical results on intermediate shocks. One of the intermediate shocks is preceded and followed by rarefaction regions with the particular property that the normal plasma velocity is equal to a normal characteristic speed at the points where the rarefactions are attached to the shock. This result constitutes the first clear occurrence of a 1=2–3=4 shock in 2D simulations. The presence of this shock is a manifestation in 2D of the nonconvex nature of the MHD equations.[22,20,21] Recently it has been shown that this type of shock, embedded in a double *xt* compound wave, is present in the analytical solution of some planar one-dimensional MHD Riemann problems.[20,21]

Our simulations are simple in setup because the incoming flow is uniform and the obstructing object is a perfectly conducting cylinder. The resulting flow, however, contains a wealth of interacting MHD shocks and discontinuities. The symmetrical 2D steady state bow shock problem is well defined. These properties make this problem a challenging new test case for ideal MHD codes.

Evidence for the shock interaction effects found in our simulations should be searched for in observations of space plasmas. Bow shocks preceding planets in a low-β environment are obvious candidates.[4] Time-dependent shock propagation phenomena may show similar shock interaction effects. Field-aligned flow is probably a rather good approximation when CMEs propagate along open magnetic field lines out of the low-β inner corona of the sun. Coronagraph observations of fast CMEs seem to show the dimple effects that were found by Steinolfson and Hundhausen[9–11] and that are also present in our simulations. The separation of the V-shaped shock front (Fig. 2) from the leading front divides the downstream flow into two distinct lobes separated by a density depletion in the V-shaped region. This feature provides a possible explanation for the double-loop appearance of some observed fast CMEs. Examination of

time sequences of CMEs in white light[11] seems to show that this double-loop appearance in many cases does not originate in the form of the CME low in the corona, but does develop in the course of the CME propagation in the outer corona. This evolution is suggestive of the possible time-dependent formation of the V-shaped shock complex found in our simulation. Further investigation of existing data or new observations with higher resolution may reveal the detailed features of our simulation results in coronagraph observations of fast CMEs. Furthermore, *in-situ* satellite observations[36] could reveal consecutive passage of fast and intermediate shocks, which could be part of a flow topology similar to the topology of our simulation results.

ACKNOWLEDGMENTS

This work derives from the Ph.D. thesis research of HDS carried out at the High Altitude Observatory, National Center for Atmospheric Research, Boulder, Colorado, USA, and at the Center for Plasma Astrophysics, K. U. Leuven, Belgium. H.D.S. acknowledges helpful discussions with A. Hundhausen, R. S. Myong, and H. Deconinck. H.D.S. was supported by a HAO Newkirk Research Assistantship. The National Center for Atmospheric Research is sponsored by the National Science Foundation (USA).

[1]S. M. Petrinec and C. T. Russell, Space Sci. Rev. **79**, 757 (1997).
[2]C. C. Wu, Geophys. Res. Lett. **19**, 87 (1992).
[3]T. Tanaka, J. Geophys. Res. **98**, 17 251 (1993).
[4]R. S. Steinolfson and S. Cable, Geophys. Res. Lett. **20**, 755 (1993).
[5]T. I. Gombosi, K. G. Powell, and D. L. De Zeeuw, J. Geophys. Res. **99**, 21 525 (1994).
[6]S. Cable and R. S. Steinolfson, J. Geophys. Res. **100**, 21 645 (1995).
[7]T. J. Linde, T. I. Gombosi, P. L. Roe, K. G. Powell, and D. L. De Zeeuw, J. Geophys. Res. **103**, 1889 (1998).
[8]C. F. Kennel, R. D. Blandford, and P. Coppi, J. Plasma Phys. **42**, 299 (1989).
[9]R. S. Steinolfson and A. J. Hundhausen, J. Geophys. Res. **95**, 6389 (1990).
[10]R. S. Steinolfson and A. J. Hundhausen, J. Geophys. Res. **95**, 20 693 (1990).
[11]A. J. Hundhausen, in *The Many Faces of the Sun*, edited by K. T. Strong, J. L. R. Saba, B. M. Haisch, and J. T. Schmelz (Springer-Verlag, New York, 1998), pp. 143–200.
[12]J. E. Anderson, Ph.D. thesis, Massachusetts Institute of Technology, 1963.
[13]M. A. Liberman and A. L. Velikovich, *Physics of Shock Waves in Gases and Plasmas*, Vol. 19 of Springer Series in Electrophysics (Springer-Verlag, Berlin, 1985).
[14]C. C. Wu, J. Geophys. Res. **95**, 8149 (1990).
[15]C. F. Kennel, R. D. Blandford, and C. C. Wu, Phys. Fluids B **2**, 253 (1990).
[16]C. C. Wu, in *Viscous Profiles and Numerical Methods for Shock Waves*, SIAM Proceedings Series, edited by M. Shearer (SIAM, Philadelphia, 1991), pp. 209–236.
[17]H. Freistuehler, J. Geophys. Res. **96**, 3825 (1991).
[18]C. C. Wu, J. Geophys. Res. **100**, 5579 (1995).
[19]H. Freistuehler and P. Szmolyan, SIAM (Soc. Ind. Appl. Math.) J. Math. Anal. **26**, 112 (1995).
[20]R. S. Myong and P. L. Roe, J. Plasma Phys. **58**, 485 (1997).
[21]R. S. Myong and P. L. Roe, J. Plasma Phys. **58**, 521 (1997).
[22]M. Brio and C. C. Wu, J. Comput. Phys. **75**, 400 (1988).
[23]J. P. Goedbloed and A. Lifshitz, Phys. Plasmas **4**, 3544 (1997).
[24]R. J. Leveque, *Numerical Methods for Conservation Laws*, Lectures in Mathematics ETH, Zurich (Birkhauser-Verlag, Basel, 1992).
[25]H. De Sterck, S. Poedts, and J. P. Goedbloed, J. Plasma Phys. **59/2**, 277 (1998).
[26]G. Fóth and D. Odstrcil, J. Comput. Phys. **128**, 82 (1996).
[27]A. A. Barmin, A. G. Kulikovskiy, and N. V. Pogorelov, J. Comput. Phys. **126**, 77 (1996).
[28]P. L. Roe and D. S. Balsara, SIAM (Soc. Ind. Appl. Math.) J. Appl. Math. **56**, 57 (1996).
[29]J. J. Quirk, Int. J. Numer. Methods Fluids **18**, 555 (1994).
[30]J. U. Brackbill and D. C. Barnes, J. Comput. Phys. **35**, 426 (1980).
[31]G. B. Whitham, *Linear and Nonlinear Waves*, *Wiley-Interscience* (Wiley, New York, 1974).
[32]J. K. Chao, Adv. Space Res. **15**, 521 (1995).
[33]C. C. Wu and C. F. Kennel, Phys. Rev. Lett. **68**, 56 (1992).
[34]C. C. Wu and C. F. Kennel, Geophys. Res. Lett. **19**, 2087 (1992).
[35]H. Karimabadi, Adv. Space Res. **15**, 507 (1995).
[36]N. R. Sheeley, Jr., R. A. Howard, D. J. Michels, M. J. Koomen, R. Schwenn, K. H. Muehlhaeuser, and H. Rosenbauer, J. Geophys. Res. **90**, 163 (1985).